Human Molecular Genetics, 2012, Vol. 21, No. 8 **1706–1724**
doi:10.1093/hmg/ddr605
Advance Access published on December 23, 2011

Myofibrillar myopathy caused by a mutation in the motor domain of mouse MyHC IIb

Ramakrishna Kurapati[1], Caoimhe McKenna[2], Johan Lindqvist[3], Debbie Williams[1], Michelle Simon[1], Emily LeProust[5], Jane Baker[1], Michael Cheeseman[1], Natalie Carroll[4], Paul Denny[1], Steve Laval[2], Hanns Lochmüller[2], Julien Ochala[3] and Gonzalo Blanco[4,*]

[1]MRC Mammalian Genetics Unit, Harwell OX11 0RD, UK, [2]Institute of Human Genetics, International Centre for Life, Newcastle upon Tyne NE1 3BZ, UK, [3]Department of Neuroscience, Uppsala University, Uppsala 751 85, Sweden, [4]Biology Department, University of York, York YO10 5DD, UK and [5]Genomics Research & Development, Agilent Technologies Inc, 5301 Stevens Creek Boulevard, Santa Clara, CA 95051, USA

Received November 16, 2011; Revised and Accepted December 15, 2011

***Ariel* is a mouse mutant that suffers from skeletal muscle myofibrillar degeneration due to the rapid accumulation of large intracellular protein aggregates. This fulminant disease is caused by an ENU-induced recessive mutation resulting in an L342Q change within the motor domain of the skeletal muscle myosin protein MYH4 (MyHC IIb). Although normal at birth, homozygous mice develop hindlimb paralysis from Day 13, consistent with the timing of the switch from developmental to adult myosin isoforms in mice. The mutated myosin ($MYH4^{L342Q}$) is an aggregate-prone protein. Notwithstanding the speed of the process, biochemical analysis of purified aggregates showed the presence of proteins typically found in human myofibrillar myopathies, suggesting that the genesis of *ariel* aggregates follows a pathogenic pathway shared with other conformational protein diseases of skeletal muscle. In contrast, heterozygous mice are overtly and histologically indistinguishable from control mice. $MYH4^{L342Q}$ is present in muscles from heterozygous mice at only 7% of the levels of the wild-type protein, resulting in a small but significant increase in force production in isolated single fibres and indicating that elimination of the mutant protein in heterozygotes prevents the pathological changes observed in homozygotes. Recapitulation of the L342Q change in the functional equivalent of mouse MYH4 in human muscles, MYH1, results in a more aggregate-prone protein.**

INTRODUCTION

Myofibrillar myopathies (MFMs) comprise a group of spontaneous and familial muscle disorders characterized by common morphological features, namely the disintegration of the myofibrillar network and the accumulation of protein aggregates containing desmin and other proteins. The majority of myofibrillar myopathy cases remain genetically undetermined (1). However, the presence of heterogeneous intracellular aggregates and the fact that most known causative mutations are missense mutations have led to the postulation that the primary molecular event in myofibrillar myopathies is likely to be a protein conformational change (2). So far, mutations have been found in components of the sarcomeric Z-disc, including FHL1, ZASP, FilaminC, Myotilin, BAG3, α/β Crystallin, plectin and desmin (for recent reviews, see 1–4). It could be expected that other sarcomeric proteins will be identified with the functional capacity to provoke similar pathological changes that are not necessarily restricted to the sarcomeric Z-disc. Indeed, mutations in the skeletal muscle myosin genes *MYH2* (coding for MyHC IIa) and *MYH7* (coding for MyHC I) have been reported, which also result in the accumulation of intracellular aggregates that contain ubiquitin and α/β crystallin (5–7). Most cases followed a dominant mode of inheritance of a missense mutation. Thus, a mutation in MYH2 (Glu706Lys) causes a dominant form of congenital myopathy (6,7), which was considered to be a variant of hereditary inclusion body myopathy (hIBM3) (8). The Arg1845Trp change within the rod domain of myosin MyHC I (*MYH7)*, which has been identified in

*To whom correspondence should be addressed at: Biology Department, University of York, Heslington, York YO10 5DD, UK. Tel: +44 1904328593; Email: gonzalo.blanco@york.ac.uk

© *The Author 2011. Published by Oxford University Press. All rights reserved.*
For Permissions, please email: journals.permissions@oup.com

Downloaded from https://academic.oup.com/hmg/article/21/8/1706/621832 by guest on 13 March 2024

independent families, also causes a dominant form of myosin storage myopathy (9,10). Because of the presence of intracellular protein aggregates, these so-called myosinopathies have also been grouped together with MFMs under the general term of protein aggregate myopathies (PAMs) (11).

Establishing genotype-phenotype correlations for myosin mutations is a challenging exercise. For example, the pattern and effects of mutations in MyHC I is complex, with mutations in the rod domain of MyHC I being recessive or dominant and leading to different phenotypic outcomes: the Glu1883Lys change causes recessive myosin storage myopathy with cardiomyopathy (12) while the Ala1379Thr change causes dominant hypertrophic cardiomyopathy without reported skeletal muscle involvement (13). However, it seems clear that accumulation of aggregated material correlates with missense mutations also in the case of myosins. The total loss of function may not result in pathogenic inclusions. Thus, recently, mutations causing the total absence of MyHC IIa have been described in compound heterozygous patients who suffer early onset myopathy, but there is no evidence of intracellular protein accumulation in inclusions or cores (14). In the mouse, no missense mutations in any of the sarcomeric myosins have been reported. However, the consequences of the total loss of function of adult skeletal muscle myosins have been characterized in detail in knockout (KO) mice for *Myh4* (MyHC IIb) and *Myh1* (MyHC IId). Again, there is no evidence of intracellular accumulation of protein inclusions in any of these mutant lines (15–18).

The objective of this work was to identify the genetic mechanism underlying the mouse mutant *ariel*, characterize its early onset myopathy and provide insights into the pathogenic mechanism. Here, we describe the identification of a recessive missense mutation in the *Myh4* gene and its consequences at cellular, physiological and pathological level in the *ariel* mouse. Our findings suggest that *ariel* suffers from a fulminant myofibrillar myopathy and add weight to the notion that, when mutated, skeletal muscle myosins can cause divergent pathological outcomes.

RESULTS

Identification of the ariel mouse mutant and the causative mutation

Ariel was identified in a third-generation (G3) *N*-ethyl *N*-nitrosourea (ENU) mutagenesis screen set up for the identification of recessive mutant alleles, involving the strains C57BL6/J (mutagenized) and C3H/HeH (non-mutagenized). *Ariel* homozygotes were recognized by the appearance of hindlimb paralysis from postnatal day 13. Initial linkage analyses using 12 homozygous mice indicated that the mutation co-segregated with C57BL6/J markers located on the distal region of mouse chromosome 11. Additional outcrosses of heterozygous mice to the non-mutagenized background C3H/HeH, followed by intercrosses of heterozygous progeny mice were set up to generate more homozygotes for high-resolution mapping. Analysis of 73 homozygous mice identified the minimal region in which the *ariel* mutation must lie between the recombinant markers rs26970400 (62.44 Mb) and rs26905080 (68.01 Mb), corresponding to a physical distance of 5.57 Mb. A next generation sequencing approach was then followed and two mutations were identified, one within the three prime untranslated region of *Pmp22* (62.9 Mb) and the other within the exon 11 of *Myh4* (67.1 Mb). The *Pmp22* mutation was ruled out through further breeding and analysis of recombinant mice, which established that marker rs3714311 (64.08 Mb) was a proximal recombinant maker, therefore leaving *Pmp22* outside of the non-recombinant interval. There was no difference at phenotypic and histopathological level between mice showing the *Pmp22* and *Myh4* mutation and those showing only the *Myh4* mutation. The mutation in *Myh4*, an A/T→T/A transversion confirmed in all homozygous mice tested (Fig. 1A), provokes a change from leucine (hydrophobic) to glutamine (hydrophilic) at position 342 within the myosin head motor domain. The leucine 342, located at the end of an a-helix, is conserved in all skeletal and cardiac muscle myosin heavy-chain isoforms identified (MYH1, MYH2, MYH3, MYH4, MYH6, MYH7, MYH8 and MYH13) and in other skeletal myosins from different species (Fig. 1B and C). The proteolytic digestion of myosin produces a soluble fragment of ∼120 000 Da denominated S1, which contains all the enzymatic activity of myosin and is able to transport actin *in vitro* motility assays (19). The S1 fragment produces upon limited proteolysis three fragments named after their apparent molecular masses: 25K (N terminal), 50K (middle) and 20K (C terminal) (20). The 50K fragment spans two domains: the 50K upper domain and the 50K lower domain or actin-binding domain. The position of the mutation within the 3D structure of the skeletal muscle myosin subfragment S1 from chicken [PDB ID: 2MYS (21,22)] is shown in Figure 1D. The L342Q mutation can be further localized in the upper 50 K domain. Based on the genetic evidence and the subsequent functional analysis described below, we conclude that this change is pathogenic. Consequently, we refer here to the mutant allele and corresponding protein as $Myh4^{arl}$ and $MYH4^{L342Q}$, respectively.

Histopathology of $Myh4^{arl}$/ $Myh4^{arl}$ mice

Homozygous *ariel* mice ($Myh4^{arl}/Myh4^{arl}$) are indistinguishable from control mice from birth to postnatal day 11, as determined by total weight and cross sections of hindlimb muscles (data not shown). From day 11, homozygous mice show a rigid gait with elevated pelvis, quickly progressing to complete hindlimb paralysis by Day 13. Examination of 23 different tissues (see Materials and Methods for details) at Day 12 indicated that skeletal muscle was the only tissue displaying pathological changes. No other organ pathology was evident. Muscle groups from the hind and forelimbs, the vertebra and the hip were markedly atrophic and typified by perivascular and perimysial inflammation (see a comparative lower hindlimb cross section in Fig. 2A and detail in B). Fast muscles are largely affected (tibialis anterior, extensor digitorum longus, peroneus longus, gastrocnemius lateralis and gastrocnemius medius), consistent with the high proportion of MyHC IIb fibres in these tissues. Conversely, diaphragm and soleus are mostly unaffected, consistent with MyHC IIb being only marginally expressed in these muscles in young and adult mice (23) (compare the normal appearance of soleus, identified by IHC with anti-MYH7 antibodies, to the adjacent highly nucleated

Downloaded from https://academic.oup.com/hmg/article/21/8/1706/621832 by guest on 13 March 2024

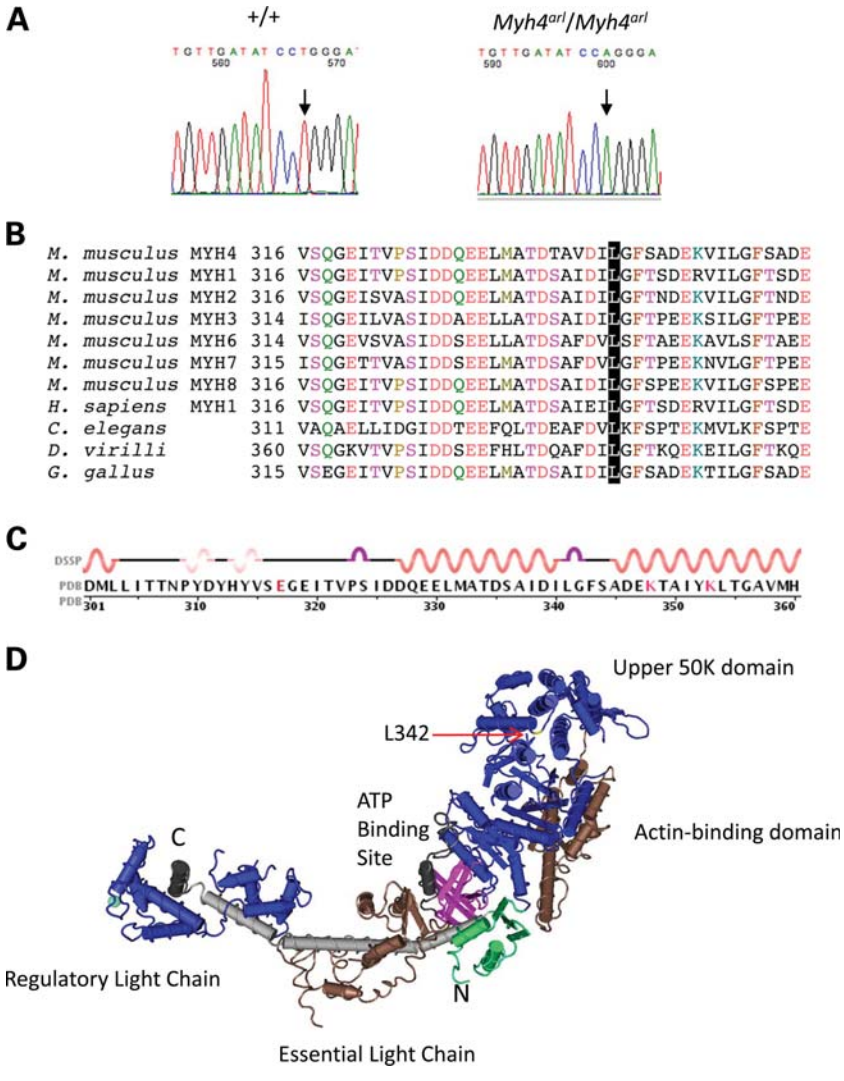

Figure 1. Identification of the *ariel* mutation within the motor domain of MYH4. (**A**) Sequencing traces of a fragment of the *Myh4* gene from a control (+/+) and a homozygous ($Myh4^{arl}/Myh4^{arl}$) showing replacement of a 'T' by an 'A' (arrows). (**B**) Multiple alignment of mouse, human, *Caenorhabditis elegans* and *Drosophila* muscle myosins (accession numbers from top: NP_034985, NP_109604, NP_001034634, NP_001093105, NP_034986, NP_542766, P12882, NP_796343, NP_492053, XP_002051993 and pdb2mys). Pdb2mys corresponds to chicken myosin (protein database identifier DOI:10.2210/pdb2mys/pdb) and provides the secondary and three-dimensional structures shown below. The residue mutated in MYH4 in *ariel*, Leucine 342, is highlighted. Amino acids are colour-coded according to their chemical properties. (**C**) Predicted secondary structure of the region containing the Leucine 342 residue from pdb2mys. Note that the residue equivalent in this sequence to L342 in mouse MYH4 resides at the end of an alpha-helix (annotations of the coloured line as follows: orange: alpha-helix; magenta: hydrogen bond turn; pink: 3-helix; black: bend), from the Protein Data Bank and according to (43). (**D**) A cartoon model using cylindrical helices of the S1 region of chicken myosin generated using pdb2mys and the Cn3D software (44). Proteolytic domains (see text) and the light chains have been arbitrarily coloured to facilitate identification and are annotated according to (22). The location of Leucin 342 within the upper 50K proteolytic domain is identified with a red arrow. N and C denote N- and C-terminal ends of the protein, respectively.

gastrocnemius in Fig. 2A). Staining of longitudinal sections with phosphotungstic acid haematoxylin (PTAH) showed evidence of myofibrillar degeneration and accumulation of intracellular protein aggregates, which can occupy almost the full diameter of the muscle fibres (Fig. 2C). The features observed in *ariel* homozygotes contrast with the lack of changes in heterozygotes. Heterozygous mice did not show any difference in weight or observed gait when compared with control mice. Moreover, analysis of H&E stained hindlimb muscle sections from young and 6-month-old heterozygous mice ($Myh4^{arl}/+$) did not show any pathological change or cross-sectional size difference compared to control mice (data not shown).

Expression of myosins in ariel homozygotes

The onset and distribution of the *ariel* pathology correlates well with the timing of the postnatal switch of MyHC isoforms from the embryonic and perinatal types to the adult isoforms, which include MYH4 (18). Since in heterozygous mice the presence of wild type MYH4 presumably prevents the pathology, the prediction is that fibres that undergo a degenerative process in homozygotes will not co-express any other skeletal muscle myosin. To test this, sections of 12 days old mice were stained with antibodies against MYH7 (type I), MYH2 (type IIa), MYH4 (type IIb) and MYH8 (perinatal) (antibody 6H1

Downloaded from https://academic.oup.com/hmg/article/21/8/1706/621832 by guest on 13 March 2024

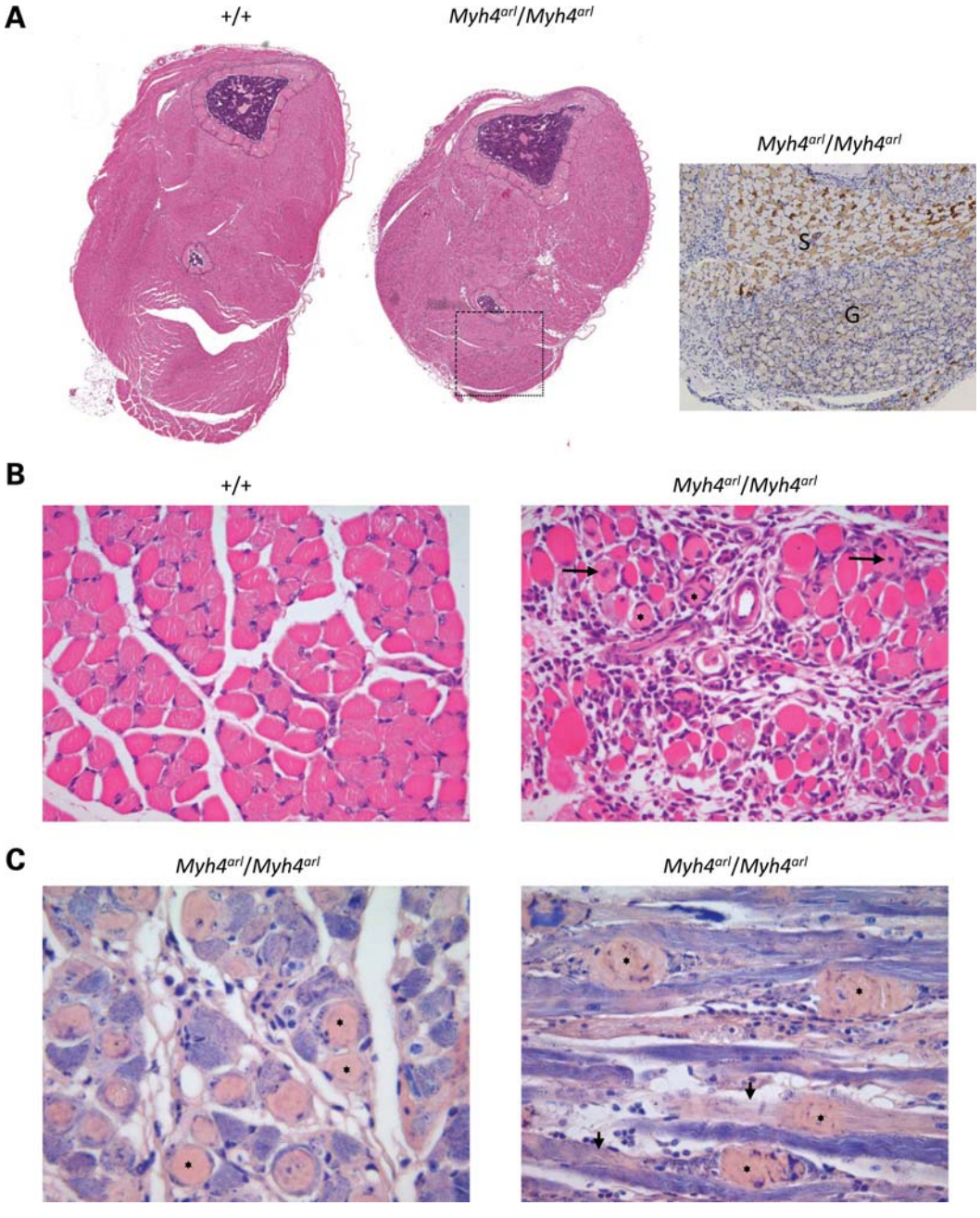

Figure 2. Representative sections of lower hindlimbs from 13-day-old mice. (**A**) H&E-stained whole limb-levelled cross section of control (+/+) and a homozygous (*Myh4*^{arl}/*Myh4*^{arl}) mice at scale; note the overall muscle atrophy of the *ariel* homozygotes. The right panel shows a DAB stain with an anti-MYH7 antibody (brown) of the region depicted by a dotted square with haematoxylin as counterstain. Note that the soleus (S), containing mainly MYH7 fibres stained in brown and unstained MYH2 fibres, shows no signs of pathology, while the adjacent gastrocnemius, rich in MYH2 and MYH4 fibres, shows marked infiltration and irregular fibre sizes. (**B**) A detailed view of H&E-stained gastrocnemius muscle from control and *ariel*. Note the regular fibre size in the control (+/+) and the degenerative changes present in the *ariel* homozygous sample, including a conspicuous inflammatory infiltration, irregular fibre size, occasional centronucleation (arrows) and pale (asterisk) as well as dark pink fibres. Pictures taken at ×400 magnification. (**C**) Phosphotungstic acid–haematoxylin stain of cross (left, ×400 magnification) and longitudinal (right, ×600 magnification) sections of the gastrocnemius muscle from a 13-day-old *ariel* homozygote. Note the sarcomeric striations on the longitudinal section stained dark blue and the presence of large intracellular aggregates stained in very light pink/brown on both sections (asterisks). Myofibrillar dilution is also noticeable in some fibres (arrows).

specific for IId/x fibres (24), failed to perform in our hands). The results showed that there was no simultaneous expression of MYH4 with any of the other myosins tested (Fig. 3). The expression and distribution of these myosins are indistinguishable from controls, with the exception of MYH8 (perinatal myosin), which is strongly expressed in scattered fibres of the hindlimb soleus/gastrocnemius region only in samples from *Myh4*^{arl}/*Myh4*^{arl} mice (Fig. 3, bottom panels). These MYH8 positive fibres did not express MYH4 and are likely to represent isolated examples of regenerating fibres. While

Downloaded from https://academic.oup.com/hmg/article/21/8/1706/621832 by guest on 13 March 2024

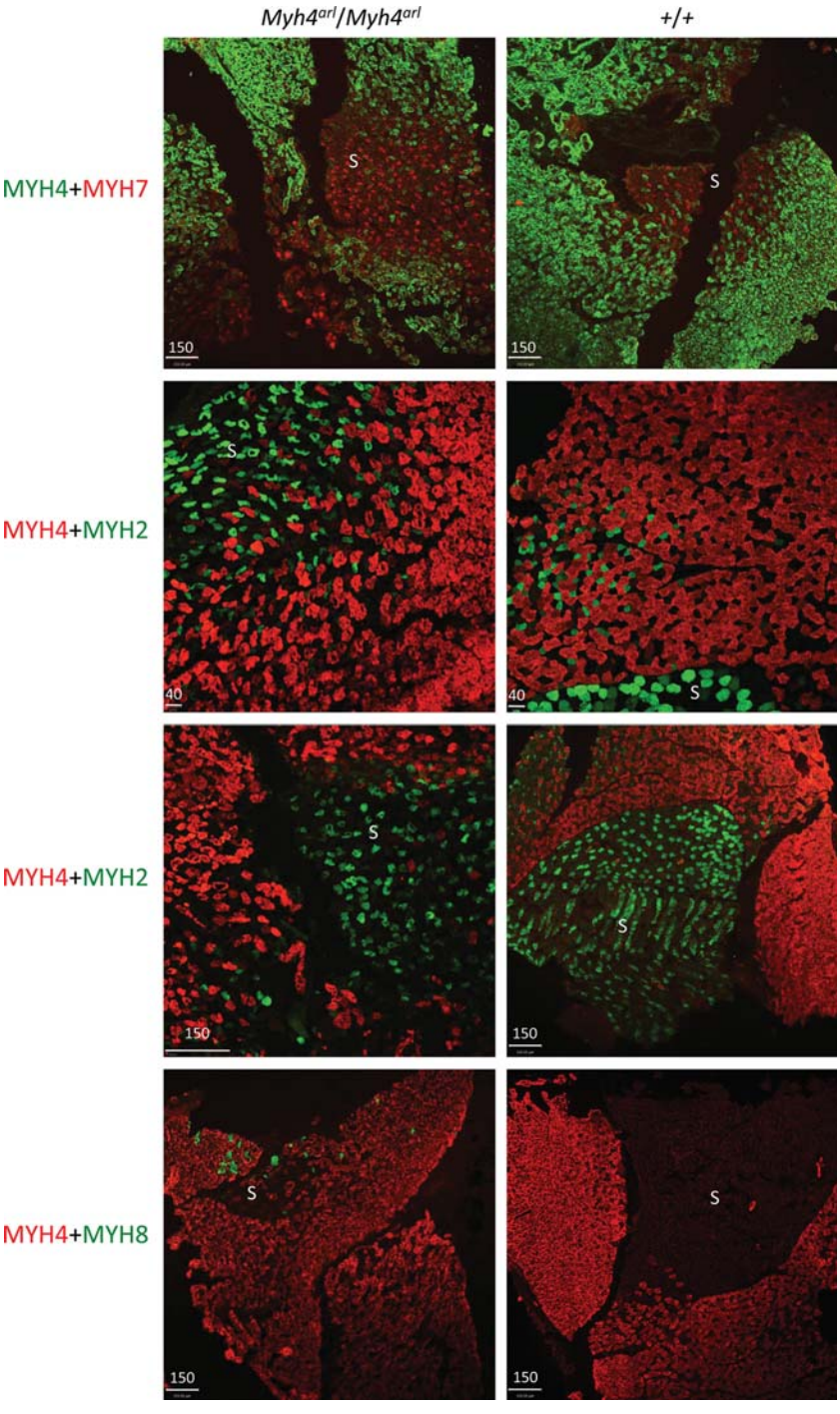

Figure 3. Immunofluorescence staining for MYH2 (type IIa), MYH4 (type IIb), MYH7 (type I) and MYH8 (neonatal) of cross sections from control (+/+) and homozygous ($Myh4^{arl}/Myh4^{arl}$) 12-day-old mice. The regions shown encompass soleus (S) and surrounding tissues. Size bars as indicated in mm. Each myosin is stained green or red as indicated by the colour of its name on the left side of the panels. Note that there are no examples of double-stained fibres in any of the combinations shown, indicating that only one type of myosin is predominantly expressed in each fibre.

MYH1 (IId/x) could not be analysed, there is no evidence that in homozygous mice the mutant myosin is forming heterodimers with any other myosin.

The expression analysis above suggests that the accumulation of $MYH4^{L342Q}$ in the absence of any other myosin isoform leads to the formation of intracellular aggregates, but does not prove that aggregates are the direct consequence of a gain-of-function activity of the mutant protein *in vivo*. The formation of aggregates could be secondary to the incorporation of $MYH4^{L342Q}$ to the thick filament, resulting in a non-functional filament, and eliciting a degradative process of the sarcomere. To address whether these aggregates are caused by

Downloaded from https://academic.oup.com/hmg/article/21/8/1706/621832 by guest on 13 March 2024

the direct aggregation of the mutant protein prior to sarcomere assembly or, alternatively, are the result of an inactive myosin already incorporated to the A-band, we analysed the expression of the mutant and wild-type forms in culture.

Myh4^{L342Q} fails to form thick filaments *in vivo* and *in vitro*

Full-length MYH4 and MYH4^{L342Q} were tagged with GFP at the C terminus and expressed under the control of the CMV promoter in transiently transfected COS7 cells. In this heterologous system, in which the sarcomeric cytoskeletal context is not available, transfection efficiencies were similar and both proteins produced bright inclusions, but MYH4^{L342Q}:GFP produced twice as many cells with inclusions than MYH4:GFP (see Materials and Methods for details and quantification in Fig. 4A). The propensity of the mutant protein to form inclusions might therefore prevent its ability to incorporate into thick filaments. To test this, we transiently transfected C2C12 myoblasts and induced them to differentiate. In these fully differentiated myotubes, the wild-type MYH4:GFP protein efficiently incorporated into thick filaments, while cells that were expressing the mutant form failed to differentiate and form striations (Fig. 4B). Overexpression of MYH4^{L342Q}:GFP appeared to prevent differentiation, since none of the cells showing expression after a week in a differentiation medium were multinucleated (observed in three independent transfections with MYH4^{L342Q}:GFP; $n = 46$ in the combined experiments). To test the possibility of overexpressed MYH4 rescuing the effects of MYH4^{L342Q}:GFP, a new tagged version of MYH4 was built by replacing GFP in MYH4:GFP with the tag tdTomato. Co-expression of MYH4:tdTomato and MYH4^{L342Q}:GFP in C2C12 myoblasts that were induced to differentiate resulted mainly in myotubes expressing only MYH4:tdTomato; however, isolated examples of co-localization of MYH4^{L342Q}:GFP and MYH4:tdTomato were observed (3 of 40 and 6 of 30 myotubes in two independent experiments), indicating that overexpression of both proteins partially enables MYH4^{L342Q}:GFP to incorporate into thick filaments (Fig. 4C).

To clarify whether the mutant form is able to target the thick filaments in the absence of any other MyHC isoforms, we analysed longitudinal muscle sections of *Myh4^{arl}/Myh4^{arl}* mice at Day 9/10 post-partum, when expression of MYH4 was already detectable by immunofluorescence, but myofibrillar and myofibre degeneration was not widespread. On these sections, fibres expressing MYH4^{L342Q} that contained well-preserved striations, as indicated by a-actinin staining, could readily be identified (Fig. 5). These fibres contained MYH4^{L342Q} distributed in a diffuse and punctate pattern along the length of the fibre, indicating no clear evidence of stable incorporation into thick filaments (Fig. 5A). Likewise, in fibres containing aggregates from older mice (postnatal day 13), MYH4 accumulates strongly around the insoluble inclusions without incorporating into thick filaments (Fig. 5B).

In contrast to the observations above in homozygous *ariel* mice, in heterozygous mice, MYH4^{L342Q} does not elicit the formation of aggregates and therefore must be incorporated into thick filaments. This conclusion, however, presumes that both alleles are expressed in the heterozygous mouse, a notion that was tested next.

Ariel heterozygous mice express equal amounts of transcripts but different amounts of proteins from mutant and wild-type loci

The expression of mutant and wild-type alleles in heterozygous mice was first quantified at the transcript level. Two real-time quantitative PCR assays were developed to amplify specifically either the wild-type or the mutant transcripts (see Materials and Methods for details). The results showed the specificity of the probes and indicated that in the heterozygous background both alleles were expressed at similar levels (Fig. 6). Interestingly, the levels of expression in homozygous mice ($n = 5$) were significantly lower than the total levels of expression observed in control ($n = 4$) and heterozygous mice ($n = 6$). This is likely to be caused by the acute muscle degeneration and concomitant cellular infiltration of the muscles in homozygous *ariel* mice. Such alteration of the tissue cellular composition will reduce the net contribution of a muscle-specific gene to the total RNA, since the internal control GAPDH would also be represented in other cell types, such as infiltrating macrophages (note the different cellular profiles of muscle from control and homozygous mice in Fig. 2B). Since both mutant and control *Myh4* transcripts are present at similar levels in the heterozygous mice, both proteins are expected to be present. To test this, the relative amounts of MYH4 and MYH4^{L342Q} were quantified in heterozygous mice by liquid chromatography-mass spectrometry (LC-MS). Digestion of MYH4 with a combination of trypsin and endoproteinase Glu-C generates a small peptide surrounding L342, which was deemed suitable for the quantification analysis (see Materials and Methods for details). Two isotope-labelled peptides (LMATDTAVDILGFSADEK and LMATDTAVDIQGFSADEK, corresponding to wild-type and mutant protein, respectively) were obtained. Protease-digested protein from a pulled sample of gastrocnemius muscle from heterozygous mice ($n = 6$) was spiked with both peptides and LC-MS was carried out. Addition of known amounts of the labelled peptides to the protease-digested sample from heterozygous mice provides the reference to calculate the amounts of endogenous myosin proteins. Figure 7 shows the results obtained from the muscle digest spiked with 10 fmol each of the two labelled peptides. The two peptides were clearly separated by >4 min and the MS spectra from each retention time clearly showed their doubly-protonated ions (Fig. 7F and G). The extracted ion chromatograms were integrated to provide ion intensities, from which the amounts of mutant and wild-type protein were calculated. The percentage of mutant protein was determined to be 7% (from $n = 8$ experimental replicas, standard deviation = 1%) indicating that, in contrast to the situation in homozygous mice, the mutant protein was being efficiently degraded in the muscle fibres of heterozygous mice. Since there is no evidence of intracellular inclusions in muscle fibres from heterozygous mice, the implication is that the remaining mutant protein must make it to the A band in the presence of wild-type protein, as it was also observed *in vitro*. This could not be ascertained using any currently available antibodies, as they do not distinguish MYH4 from MYH4^{L342Q}. Therefore, we asked whether the presence of the MYH4^{L342Q} in the thick filament could be detected by measuring the contractility of

Downloaded from https://academic.oup.com/hmg/article/21/8/1706/621832 by guest on 13 March 2024

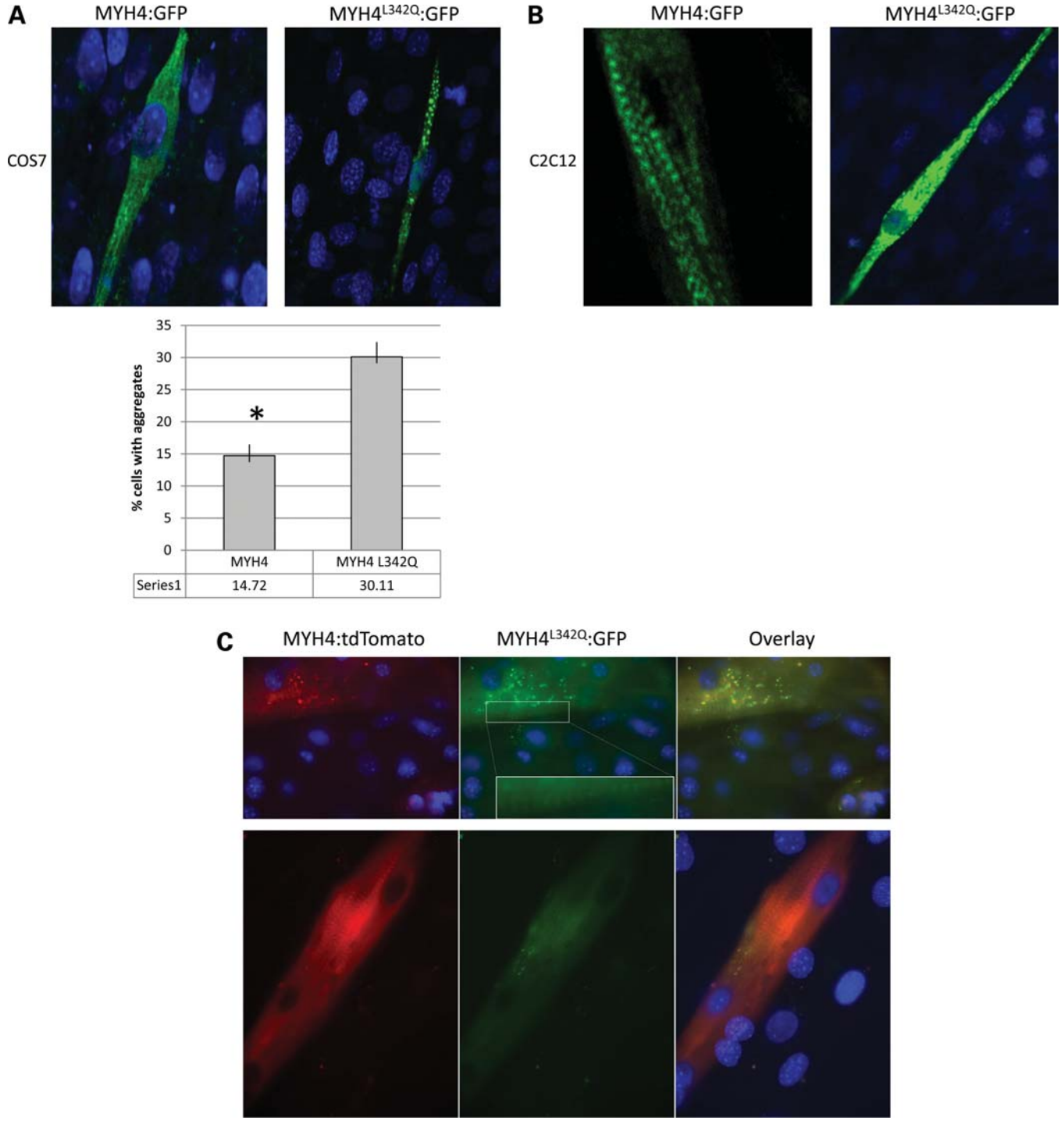

Figure 4. Overexpression of chimeric MYH4:GFP, MYH4:tdTomato and MYH4^{L342Q}:GFP on transiently transfected cells. (**A**) Examples of transfected COS7 cells with the constructs as indicated at the top of each picture. The examples shown indicate the expression patterns used to classify cells. Quantifications shown below indicate the average percentage of expressing cells that show inclusions for each construct ($n = 4$; number of expressing cells per transfection ranged from 300 to 800). Student's paired *t*-test shows that the difference is statistically significant ($P = 0.003$). (**B**) Representative examples of transiently transfected and subsequently differentiated C2C12 myoblasts using the indicated constructs. After 4 days in differentiation medium, cells transfected with MYH4:GFP fused into multinucleated myotubes showing clear A-band striations while cells transfected with MYH4^{L342Q}:GFP appear only as individual singly nucleated cells, without any evidence of striations. (**C**) Non-representative myotubes from a co-transfection of C2C12 cells with MYH4^{L342Q}:GFP and MYH4:tdTomato. The rectangles within the picture show an amplification of the region in which, in the presence of MYH4:tdTomato, weak expression of MYH4^{L342Q}:GFP at the A band can be observed.

Downloaded from https://academic.oup.com/hmg/article/21/8/1706/621832 by guest on 13 March 2024

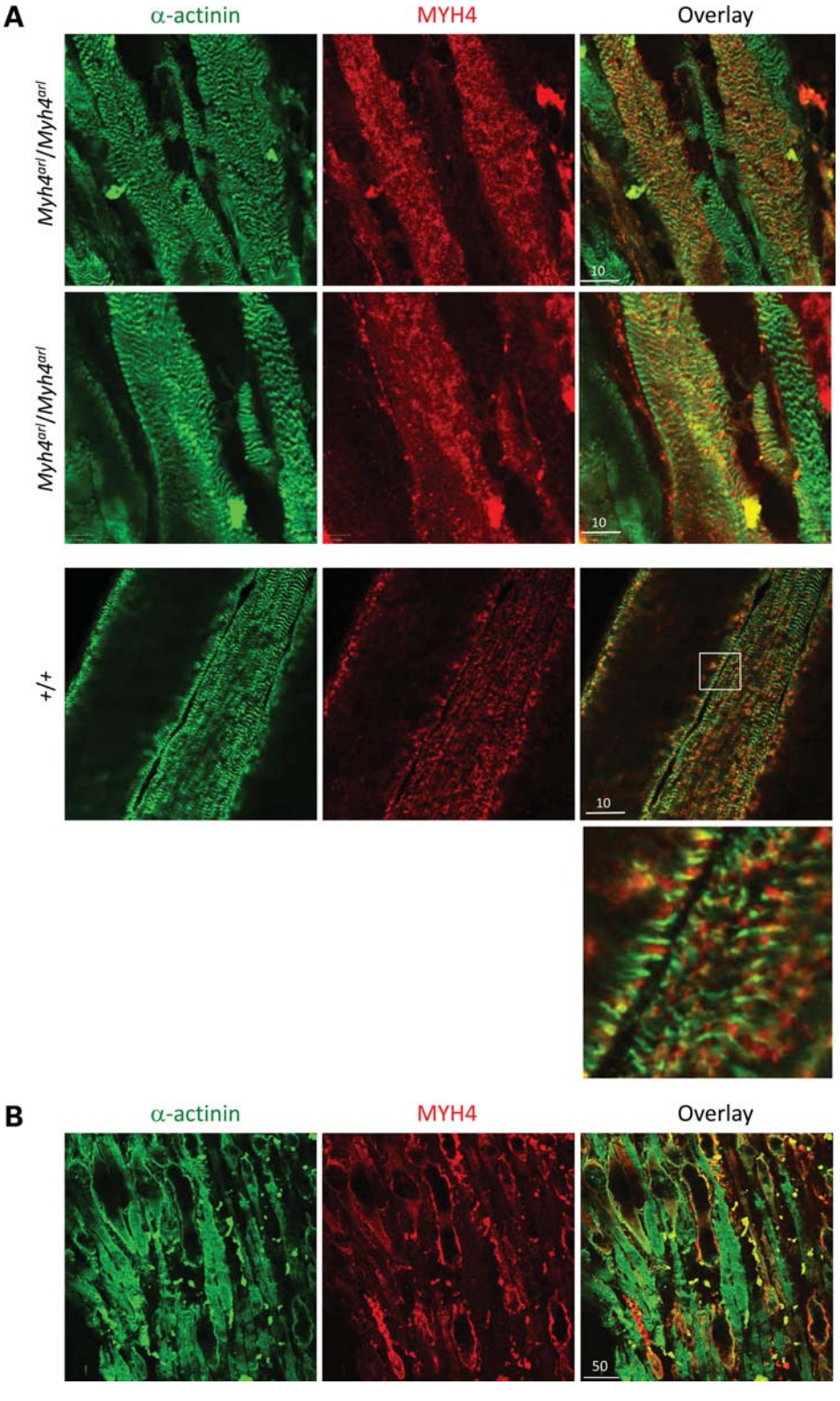

Figure 5. MYH4^{L342Q} does not form thick filaments *in vivo*. (**A**) Immunofluorescence analysis of longitudinal sections of 9- or 10-day-old *Myh4*^{arl}/*Myh4*^{arl} mice with antibodies against α-actinin (green) and MYH4 (red). Note that despite the presence of a preserved sarcomeric cytoskeleton, as indicated by the Z-band staining, MYH4^{L342Q} presents a punctate pattern and does not show clear evidence of correct sarcomeric localization. An unaffected litter mate (+/+) shows MYH4 alternating for the most part with α-actinin. At the bottom, the detail of the region indicated by a white square. (**B**) The same immunofluorescence stains as above on a 13-day-old *Myh4*^{arl}/*Myh4*^{arl} mouse showing well-developed aggregates (unstained rounded regions, marked with white asterisks). Note that MYH4 also fails to show clear evidence of a banding pattern, preferentially accumulating at this stage around the aggregates. Note that the confocal section shows the core of the aggregate unstained for MYH4 and a-actinin, but see also Figure 9. Scale bars as indicated in mm.

Downloaded from https://academic.oup.com/hmg/article/21/8/1706/621832 by guest on 13 March 2024

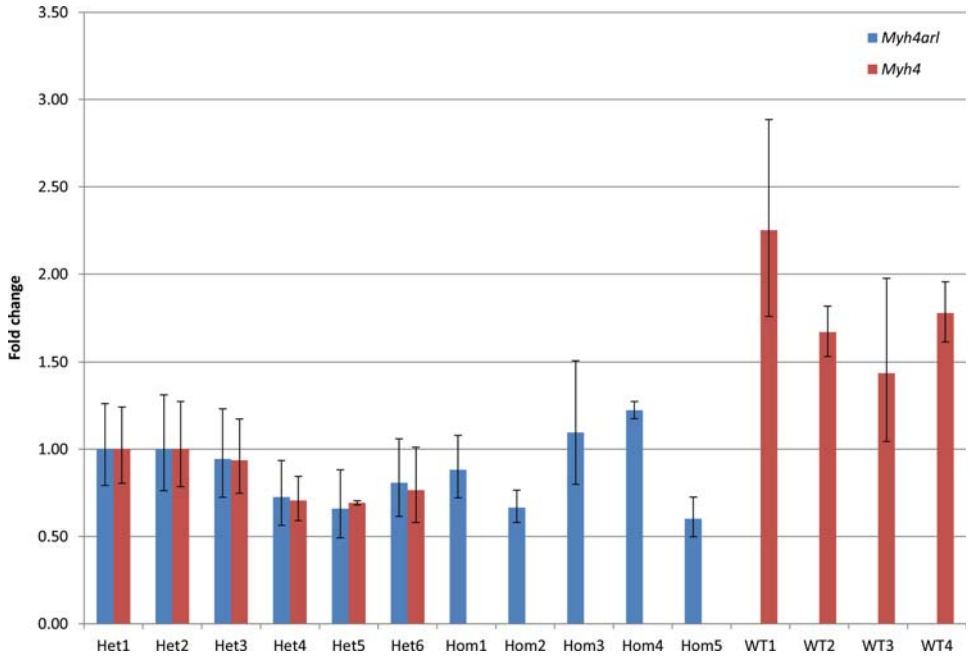

Figure 6. Expression analysis by qPCR of *Myh4*^{arl} (mutant allele, red bars) and *Myh4* (control allele, blue bars) from gastrocnemius muscles from individual mice. Genotypes: +/+ (WT1-4), *Myh4*^{arl}/+ (Het1-6) and *Myh4*^{arl}/*Myh4*^{arl} (Hom1-5). See text and Material and Methods for details.

single-membrane permeabilized fibres. Interestingly, we observed an increase in maximal force production in fibres carrying the mutant ($n = 39$) when compared with control fibres ($n = 43$) (25.96 ± 1.17 versus 21.35 ± 1.03 N cm^{-2}). We also noticed a trend towards a slower rate of force development, but this did not meet the statistical significance (33.85 ± 2.54 versus 39.39 ± 3.10 s^{-1}). These suggest an enhanced myosin binding to actin in the presence of MYH4L342Q without clear kinetics changes. This change in the contractile properties of heterozygous fibres reflects the presence of the mutant myosin form in the thick filaments and indicates that the mutant protein contributes to the myofibrillar apparatus in the heterozygous mouse.

Structural and biochemical analysis of protein aggregates

One remarkable aspect of the *ariel* mutant is how quickly the aggregates form. Aggregates are not detected at any point earlier than postnatal day 10 on sections stained with PTH (data not shown). To get an insight into the process of aggregate formation in homozygous mice, we analysed samples from young (Day 7) and symptomatic (Days 10 and 14) mice at the ultrastructural level. Samples from young homozygotes did not show any evidence of intracellular aggregates (data not shown), while samples from symptomatic animals displayed a variety of aggregate sizes, from those spanning across a few myofibrils to those spanning almost the full diameter of the fibre (a presumed 'young' aggregate is shown in Fig. 8A). The diverse structures found within aggregates indicate that they are not just misfolded mutant myosin. Aggregates contained mainly disorganized filamentous and granular material, embedded within apparently well-structured sarcomeres, which appear to dissolve in the vicinity of the aggregate (see Fig. 8B and C). From these observations, it would appear that the filamentous material of the aggregates originates from the progressive disorganization of the myofibrils rather than synthesized *de novo* (see detail in Fig. 8E and F). In addition, the lack of membrane fragments around forming aggregates suggests that these aggregates are not incorporated into lysosomes. To complement this analysis, the proteomic content of the aggregates was analysed. Since aggregates were readily detectable on cross sections, they could be purified by laser capture microdissection (Fig. 9A shows a view of a fresh-frozen section using DIC optics and decoration of the surface of the aggregates with anti-MYH4 antibodies). The proteomic contents of the aggregates (Supplementary Material, List 1) and randomly picked microdissections from wild-type muscle sections (Supplementary Material, List 2) were obtained (see Materials and Methods for details). The results have been summarized in Table 1, which contain a non-redundant list from *ariel* aggregates, which have been cross referenced to the control list. As indicated in Table 1, a number of proteins were found present only in the aggregates. Interestingly, several of these unique proteins have been found mutated or accumulated in myofibrillar myopathy, including heat shock proteins, ubiquitins, filamin C, ZASP, PDZ and LIM domain protein 3 and tubulins. As expected, some proteins highly expressed in skeletal muscle were found in both lists, including MYH4 and desmin. However, desmin, a muscle-specific intermediate filament protein, has a higher score in the aggregate list (score 448 in list from *ariel* aggregates; score 82 in control list), consistent with this protein being an ubiquitous component of many myofibrillar myopathy aggregates (25). We noted the absence of α/β crystallin, a small heat shock protein with chaperon activity, from Table 1. Since α/β crystalline has

Downloaded from https://academic.oup.com/hmg/article/21/8/1706/621832 by guest on 13 March 2024

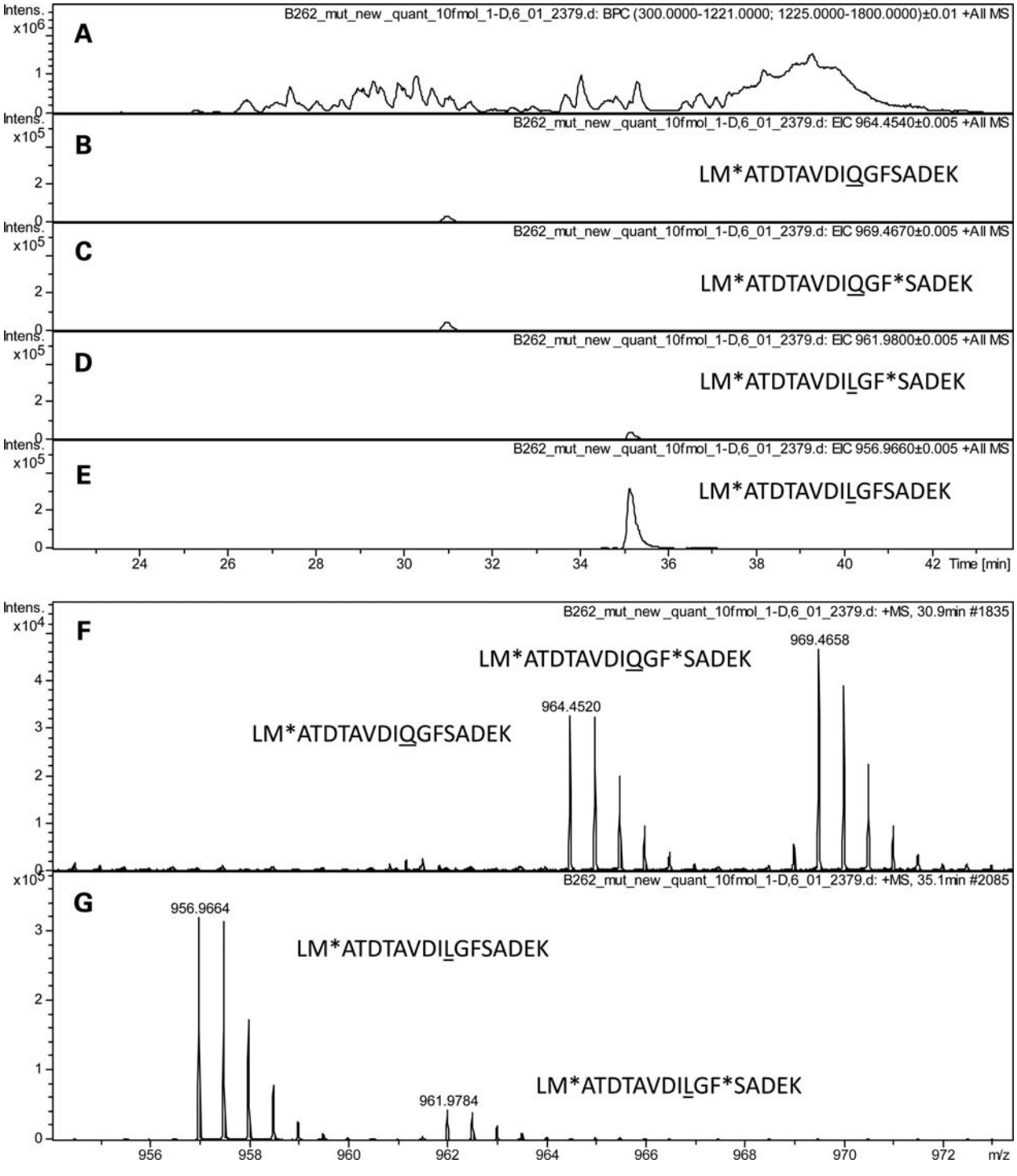

Figure 7. LC-MS of peptides produced from muscle protein by digestion with trypsin and Glu-C and spiked with stable-isotope-labelled standards. The example shown is a muscle digest with 10 fmol of each synthetic peptide added. (**A**) The base-peak chromatogram. (**B**–**E**) Extracted-ion chromatograms of *m/z* values 964.454, 969.467, 961.980 and 956.966 corresponding to the doubly protonated peptides LM*ATDTAVDIQGFSADEK, LM*ATDTAVDIQGF*SADEK, LM*ATDTAVDILGF*SADEK, LM*ATDTAVDILGFSADEK, respectively. M* denotes oxidized methionine and F* denotes [$U^{13}C_9$, ^{15}N]-labelled phenylalanine, which introduces a nominal mass increase of 10 Da. (**F**) Mass spectrum obtained at an HPLC retention time of 30.9 min containing doubly protonated ions from the native and labelled mutant peptide LMATDTAVDIQGFSADEK. (**G**) Spectrum obtained at 35.1 min containing the native and labelled wild-type peptide LMATDTAVDILGFSADEK. MYH4 amino acid residue 342 is underlined.

been found mutated in myofibrillar myopathies, where late-onset desmin-positive granulofilamentous aggregates have been described (26,27), we decided to test the presence of this protein by immunofluorescence. Immunofluorescence analysis of *ariel* homozygous sections with anti-α/β crystalline antibodies strongly labelled the aggregates (Fig. 9B).

Downloaded from https://academic.oup.com/hmg/article/21/8/1706/621832 by guest on 13 March 2024

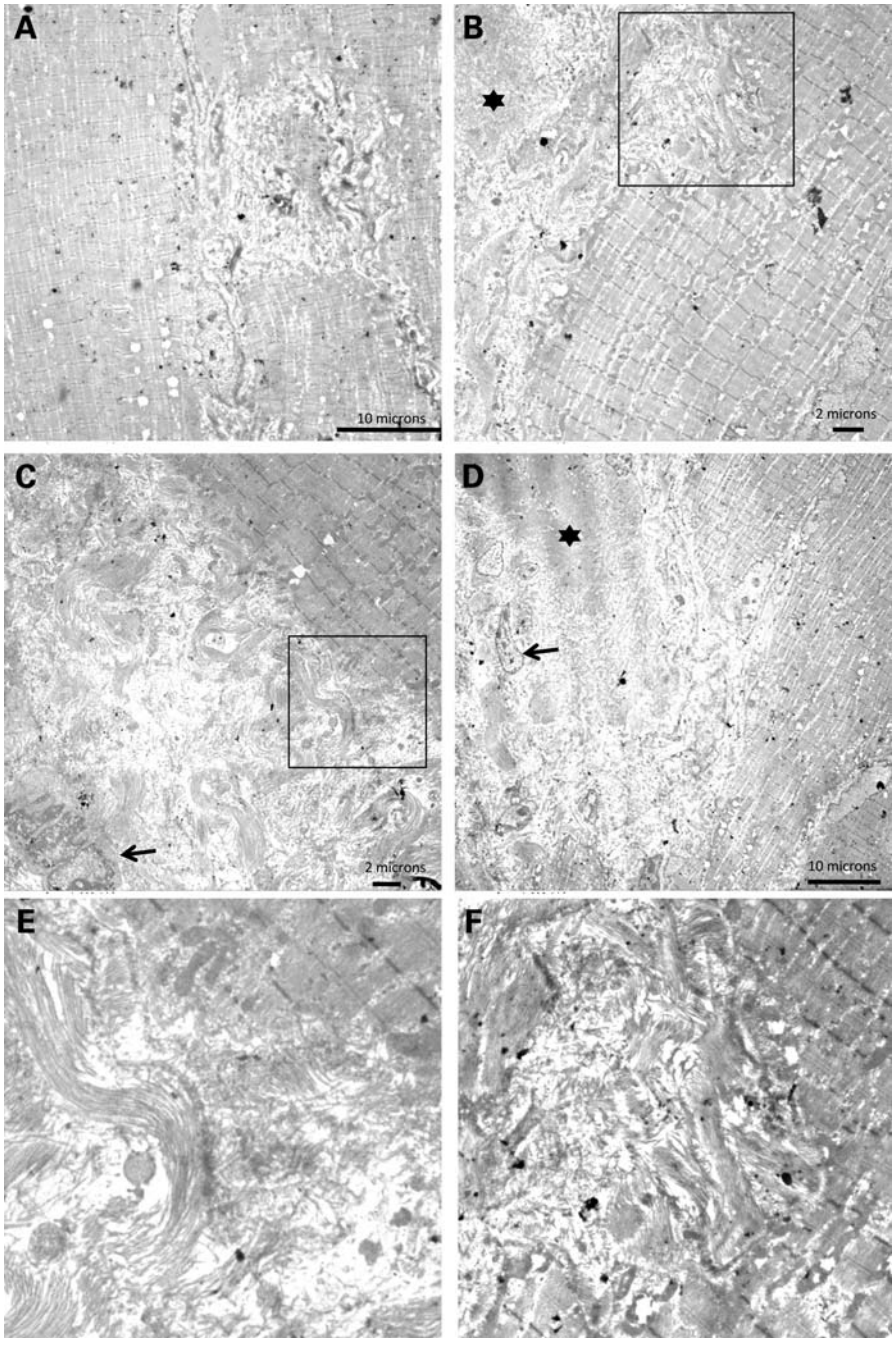

Figure 8. Representative electron microscopy pictures of *ariel* homozygotes. At Day 10 (**A**), very few aggregates are observed but focal disorganization of the myofibrils is already apparent. The aggregates grow rapidly and by Day 14 (**B**–**D**), abundant filamentous material is evident (C). The presence of granulose regions within the aggregates [asterisks in (B) and (D)] and nuclear fragments (arrows) are also common findings. The square in (B) and (C) indicate the selected region amplified in (F) and (E), respectively, showing filaments within the aggregates and flanking sarcomeres disorganizing.

Thus, while the reasons why crystalline peptides failed to be detected in the proteomic experiment are unclear, this protein is also expressed ectopically in *ariel* aggregates.

Recreation of the L342Q change in human MYH1

In mice, type IIb fibres express MyHC IIb (MYH4); in humans, only the MyHC-IIx/d isoform (MYH1) is present (28). The conservation of the mutated residue in *ariel* in all skeletal muscle myosins (Fig. 1B) suggests that an identical substitution in MYH1 may also provoke misfolding of this protein. To test this, a full-length human *Myh1* cDNA was amplified and recloned to produce a GFP-tagged version of the corresponding protein. A MYH1^{L342Q}:GFP mutant version was then generated by site-directed mutagenesis. Expression in COS7 cells of MYH1:GFP or MYH1^{L342Q}:GFP produced distinctive patterns to those obtained with MYH4 (see examples in Fig. 10). Both MYH1:GFP and MYH1^{L342Q}:GFP produced

Downloaded from https://academic.oup.com/hmg/article/21/8/1706/621832 by guest on 13 March 2024

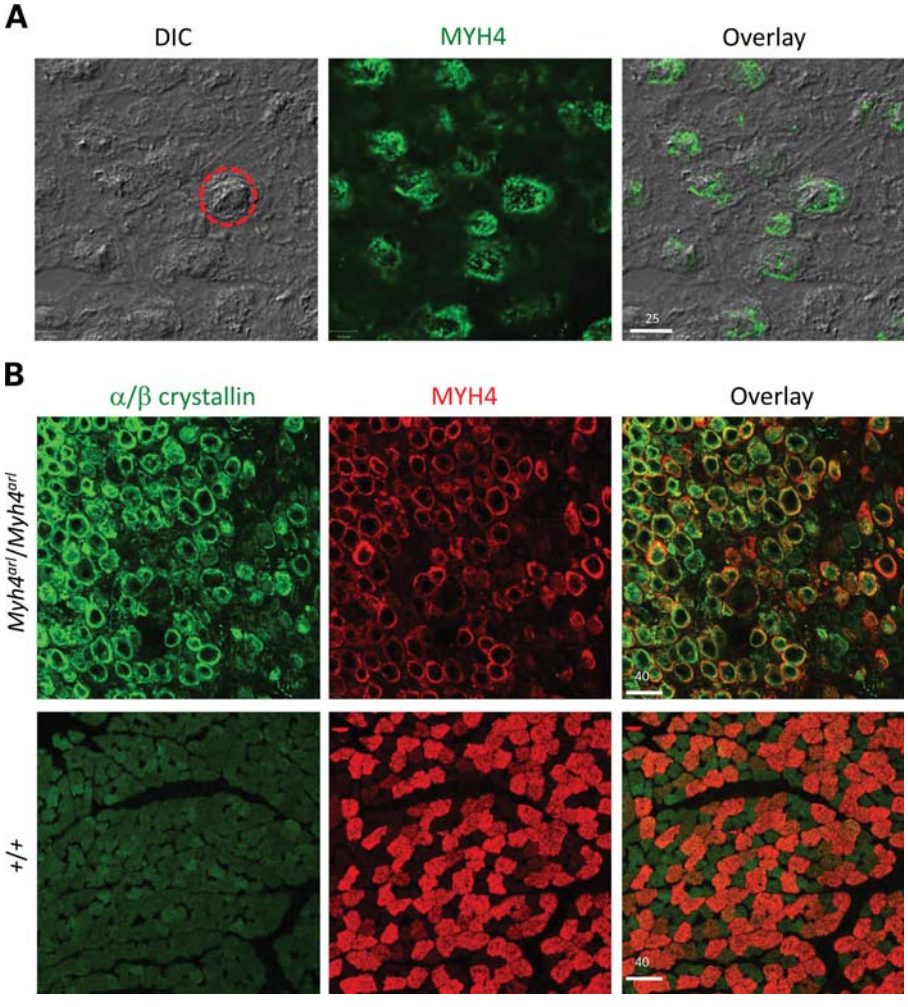

Figure 9. Characterization of *ariel* aggregates. (**A**) Ariel aggregates are very prominent and can be detected using DIC optics (example within dotted red circumference). Immunofluorescence analysis with BF-F3 antibodies shows discontinuous presence of MYH4 on the surface of the aggregates, indicating heterogeneous composition. (**B**) The presence of α/β crystallin on the aggregates was confirmed by immunofluorescence. Note also the MYH4-positive fibres show the highest expression of α/β crystallin. The confocal section cuts in some fibres through the mid-level of the aggregate, appearing dark, and in other fibres through the superficial level, where staining is then observed. Scale bars as indicated in mm.

larger aggregates than those observed previously with MYH4 and in a relatively higher number of transfected cells. However, the results of four independent transfections showed that, while the overall transfection efficiencies were similar, MYH1^{L342Q}:GFP yielded a significantly higher number of cells with aggregates than the control MYH1:GFP (an increase of 27%, see quantifications in Fig. 10).

DISCUSSION

We have established the genetic cause of a new mouse myopathy characterized by the swift degradation of type IIb fibres. The mutation identified in the *Myh4* gene was the only change found upon sequencing of all coding exons within the non-recombinant interval. The causative effect of the mutation is further supported by the time of onset, which overlaps with the timing of replacement of developmental myosins (neonatal and embryonic) by the adult isoforms (23). In fast muscles, this postnatal switch leads to the accumulation of MYH4, the most highly expressed skeletal muscle myosin in mice (29). An *Myh4* KO mouse has been generated previously and studied in detail. The loss of IIb fibres in these mice results in morphological changes in fast muscles, including interstitial fibrosis in tibialis anterior and signs of regeneration in the superficial gastrocnemius (15,17). The pathological hallmarks described in these KO mice appear to reflect a compromised adaptation of the muscle to the loss of specific fibre types, but these are mild changes compared with the fulminant muscle degeneration process observed in *Myh4*^{arl}/*Myh4*^{arl} mice, which culminate in paralyzed hindlimbs by postnatal day 13. These phenotypic differences are likely to rest on the compensatory muscle fibre hypertrophy and the secondary upregulation of the adult myosins MyHC IIa and IId in *Myh4* null mice (17). These compensatory changes do not take place in *Myh4*^{arl}/*Myh4*^{arl}. A plausible reason is that the myofibre degeneration caused by the intracellular aggregates in *ariel* homozygotes triggers an acute inflammatory process, altogether resulting in irreversible muscle wasting.

Downloaded from https://academic.oup.com/hmg/article/21/8/1706/621832 by guest on 13 March 2024

Table 1. A non-redundant list of proteins identified by mass spectroscopy from purified *ariel* aggregates

Individual ions score in ariel ($P < 0.05$)	Individual ions score in control ($P < 0.05$)	Matching protein name	gi Number
1148	1538	Myosin, heavy polypeptide 4, skeletal muscle	67189167
448	82	Desmin	33563250
240	Not found	γ-actin	809561
197	Not Found	Alpha cardiac myosin heavy chain	191618
197	211	Fast skeletal myosin alkali light chain 1	29789016
188	273	Myosin, heavy polypeptide 13, skeletal muscle	124486959
169	86	Glyceraldehyde-3-phosphate dehydrogenase	6679937
168	Not found	Muscle embryonic myosin heavy chain 3	153792649
165	119	ATP synthase, mitochondrial F1 complex	6680748
159	Not found	Similar to GAPDH	149265922
158	228	Muscle creatine kinase	6671762
154	924	Tropomyosin 2, beta	11875203
154	37	Spermatid-specific	556310
139	107	ATPase, Ca^{2+} transporting, fast twitch 1	36031132
123	Not found	Filamin C, gamma	124487139
113	Not found	Heat shock protein HSP27	424143
84	Not found	H3 histone, family 3A	4504279
80	213	Fructose-bisphosphate aldolase A	6671539
78	Not found	TI-225 Ubuiquitin C	1167510
69	Not found	mCG13235 Ubuiquitin A	148684097
68	Not found	Elongation factor 1α	50797
66	57	Enolase 3, beta muscle	6679651
63	Not found	Histone H2A	51304
61	Not found	PDZ-LIM protein cypher1c (ZASP)	11612596
58	Not found	PDZ and LIM domain protein 3	7948997
55	Not found	M2-type pyruvate kinase	1405933
52	Not found	RecName: full = Titin; AltName: full = Connectin	160358754
50	Not found	Sarcalumenin	26331358
49	Not found	Macrophage migration inhibitory factor	5542285
48	50	Myosin light chain, phosphorylatable, fast	7949078
48	Not found	Tubulin, beta, 2	5174735
43	Not found	Haemoglobin subunit alpha	122441
41	Not found	16S ribosomal protein	200796
39	Not found	Pro-alpha-2(I) collagen	50489
39	Not found	Phospholipase c	74180086
33	Not found	Cytochrome c oxidase subunit Va preprotein	50527
30	Not found	Hspa8 protein	63101351
29	Not found	Reductase superfamily containing protein	26329759
28	Not found	Malate dehydrogenase	387422

Myofibre disintegration in homozygous *ariel* mice is a consequence of the failure of the mutant protein $MYH4^{L342Q}$ to replace the neonatal isoform from the thick filaments. *In vivo* and *in vitro* expression analyses suggest that the missense mutation prevents correct protein folding. Transfected C2C12 myoblasts overexpressing control and mutant versions of MYH4 fused with GFP produced very different results. Once induced to differentiate, the control chimeric protein incorporates into thick filaments and therefore must fold correctly. The mutant chimeric protein, however, accumulates into large cytoplasmic aggregates and we failed to detect any cells progressing through differentiation, suggesting that the L342Q mutation destabilizes the native state of MYH4 and prevents maturation of the myosin complexes. Interestingly, *in vivo*, there are no inclusions present in the muscles from heterozygous mice. Weight, locomotor function or life-span is also indistinguishable from control mice (data not shown). It could be inferred that recruitment of the mutant protein to the thick filaments in the presence of the wild-type dimer is sufficient to prevent its pathogenic activity. In other words, dimerization of $MYH4^{L342Q}$ with MYH4 prevents accumulation of the former in cytoplasmic inclusions. Indeed, $MYH4^{L342Q}$ was occasionally observed to co-localize with MYH4 at the A band *in vitro* and heterozygous *ariel* mice show an enhancement of force production when measured on permeabilized single fibres, suggesting that in the presence of the wild-type dimer a fraction of $MYH4^{L342Q}$ must correctly be refolded and able to target the A band. Accurate quantification of the relative amount of proteins, however, suggests a different mechanism for the lack of effect of the *ariel* mutation in heterozygous mice. The presence of $MYH4^{L342Q}$ in the gastrocnemius from heterozygous mice was determined to be only 7% of the levels of MYH4. This huge difference in the expression levels of the proteins, despite identical transcript levels being produced, indicates that it is the effective degradation of the misfolded protein rather than its ability to dimerize with the wild-type protein, the main mechanism preventing the pathological effects of the mutation from manifesting in heterozygous mice. We speculate that the presence of normal myosin in heterozygous muscle fibres provides a physiological

Downloaded from https://academic.oup.com/hmg/article/21/8/1706/621832 by guest on 13 March 2024

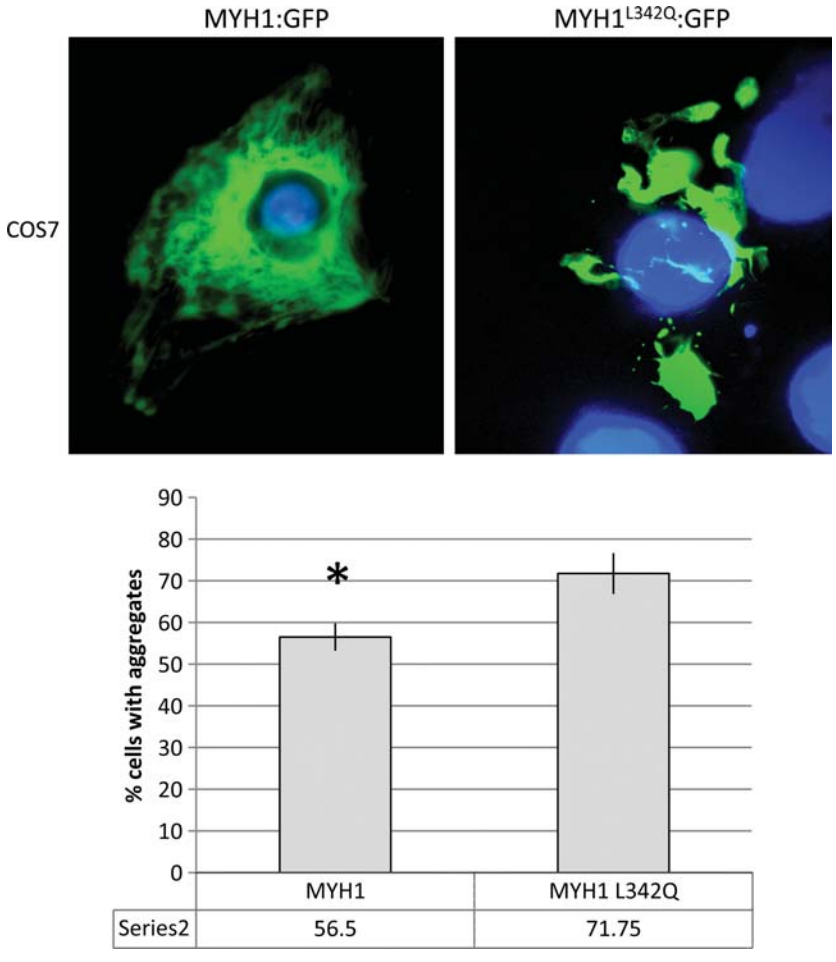

Figure 10. Over-expression of chimeric MYH1:GFP and MYH1^{L342Q}:GFP on transiently transfected cells. Examples of transfected COS7 cells with the constructs as indicated at the top of each picture. The examples shown indicate the expression patterns used to classify cells. Quantifications shown below indicate the average percentage of expressing cells that show inclusions for each construct ($n = 4$; number of expressing cells per transfection ranged from 100 to 200). Student's paired *t*-test shows that the difference is statistically significant ($P = 0.0126$).

status sufficient to deal with unfolded proteins. Conversely, the absence of any MyHC isoform within the A band of fast IIb fibres in homozygous mice results in a physiologically compromised fibre unable to deal with the accumulation of misfolded MYH4^{L342Q}.

In heterozygous mice containing a small amount of MYH4^{L342Q} in their A bands, an effect of the mutation at the actin–myosin interaction level could be expected, considering that the mutation affects a highly conserved residue within the upper 50K domain of the actin-binding domain. Upon binding to actin, the upper domain is thought to rotate to close the cleft between the upper and the lower domain, opening the nucleotide pocket on the opposite side and leading to the release of ADP (30–33). It is reasonable to suggest that some kinetics steps of the myosin cross-bridge cycle will be altered by the substitution L342Q, especially the ones related to ATP binding and dissociation. Further experiments investigating this particular point are required.

Mutations causing familial hypertrophic cardiomyopathy (FHC) in the motor or converter domain of MYH7 have been reported to result in increased force when measured in single skinned fibres from heterozygous patients (34–37). It has been suggested that the increased energy cost of the tension generation may play an important role in the pathogenesis of FHC (36). The L342Q change in MYH4 provokes a change in contractile properties that does not result in overt differences in heterozygous mice, but it would be interesting to test whether under high energy-demanding conditions, such as intensive exercise, *ariel* heterozygous mice show a myofibrillar phenotype.

To get an insight into the mechanism of aggregate formation, we studied the inclusions at ultrastructural level and analysed their protein content. Disorganized filamentous material appears to emanate from adjacent sarcomeres in early aggregates, while more developed aggregates also show large regions of granular material as well as organelle fragments. It is possible that as the turnover of myosin from embryonic/perinatal isoforms to the adult IIb isoform fails to complete, focal dissolution of the sarcomeric structures ensues resulting in disorganized filamentous material. In addition, upregulation of *Myh4* during the second postnatal week may result in increased misfolded MYH4^{L342Q} protein, attracting other proteins to the developing inclusion, which could result in the granular material observed at the ultrastructural level. While

Downloaded from https://academic.oup.com/hmg/article/21/8/1706/621832 by guest on 13 March 2024

these are merely observations that do not demonstrate the origin of the aggregated material, the presence of chaperones and other proteins typically associated with insoluble protein aggregates found in a number of MFMs suggests that the formation of *ariel* aggregates follows an overlapping pathway. Aggregates in MFM are considered to develop consequently to the failure of the extra-lysosomal pathway to deal with an unfolded protein (2). However, to our knowledge, the small temporal window over which these aggregates develop is unique to the *ariel* mutant. This may represent a valuable feature to test methods for refolding of mutant proteins, a therapeutic approach previously suggested for conformational diseases (38). Thus, preventing the formation of non-native protein oligomers in *ariel* homozygotes would facilitate the proteosomal degradation of the misfolded protein, making it more similar to the *Myh4* null, which might result in rescue of locomotor competence.

Although MYH4 is not expressed in humans at the protein level (28,39), the conservation of the mutated residue leads us to suggest that an equivalent change in those myosins expressed in human muscle may provoke a pathogenesis similar to the one described here for *ariel. In vitro*, the L342Q change increases the propensity to form aggregates of MYH4 and its human functional equivalent MYH1. Therefore, adult myosin genes should be explored as candidates for non-classified MFM patients.

MATERIALS AND METHODS

G3 screen and genetic mapping

C57BL/6J males were injected with ENU and out-crossed to C3H/HeH females to generate F1 founder males. Pedigrees were established by crossing founder males to C3H/HeH and then backcrossing F2 female offspring to their father. The *ariel* line was registered with the Mouse Nomenclature Committee (The Jackson Laboratory) (accession number MGI: 4839531). All mice were kept in accordance with UK Home Office regulations. DNA was prepared from mouse tails or ear biopsies using standard protocols. Polymerase chain reaction (PCR) amplification was carried out according to standard protocols. Low-resolution genetic mapping was carried out on *ariel* homozygous mice $Myh4^{arl}$/ $Myh4^{arl}$ progeny from $Myh4^{arl}$/+ X $Myh4^{arl}$/+ crosses on a C57BL6/J/ C3H/HeH genetic background. A small number of mice were genotyped at ~90 polymorphic microsatellite markers, spaced at ~20 cM across all chromosomes, using semi-automated fluorescent microsatellite analysis on an ABIPrism 377 DNA sequencer. Data were collected using ABIPrism 377XL DNA sequencer Data Collection (Version 2.6) software and analysed using ABIPrism GeneScan Analysis software (version 3.7.1) and ABIPrism Genotyper software (version 3.7). Linkage was established and confirmed by genotyping additional markers at the linked region. Mice that were recombinant at flanking markers were genotyped at additional annotated microsatellite and single-nucleotide polymorphism (SNP) markers within the non-recombinant region by using single-stranded conformational polymorphism analysis on 6% polyacrylamide gels analysis and biotin-labelled PCR and pyrosequencing analysis on a PSQ HS 96A pyrosequencer (Biotage), respectively.

Histological analysis

Necropsy and other tissue histology. For necropsy and other tissue analysis, mice were culled by intraperitoneal barbiturate overdose. Lungs were inflated with 10% neutral buffered formalin (NBF), leaving the heart attached. All tissues were fixed in 10% NBF with the exception of testes that were fixed in Bouin's solution and the eyes in Davidson's solution. Bony tissues were decalcified in 10% formic acid. The following tissues were fixed for histology: eyes, brain and pituitary, tongue, thyroids and parathyroids, trachea, lung, heart, esophagus, stomach, small and large intestines, pancreas, liver, kidneys and adrenals, spleen, sciatic nerve, skin samples from the nose, dorsum and ventrum, thigh muscle (semimembranosus and quadriceps), diaphragm, lumbar vertebral column, knee joint, tail foot and head, and in the male, testes and accessory reproductive glands, and ovaries and tubular genitalia in the females. Six-micrometre sections were cut and analysed for abnormalities.

Skeletal muscle immunofluorescence. Tissues from 7- to 14-day-old mice were frozen in isopentane cooled in liquid nitrogen prior to cryosectioning and then stored at −70°C. After thawing and drying, sections were used unfixed or sections were fixed with either cold acetone (pure or as a 1:1 mixture with cold methanol) or 4% paraformaldehyde for 30 min and rinsed with PBS three times. Standard indirect immunofluorescence was employed using primary rabbit and mouse monoclonal antibodies followed by FITC- or TRITC-conjugated polyclonal anti-mouse, or anti-rabbit, immunoglobulins (Sigma) and visualized using a Zeiss Axiosope fluorescent microscope or a Bio-Rad MRC 500 confocal laser scanning system attached to a Nikon Diaphot inverted microscope. The antibodies used in this work were: rabbit polyclonal anti-MYH7 (SIGMA), mouse monoclonal isotype IgG1 SC-71 against MYH2 (Hybridoma Bank, University of Iowa), mouse monoclonal isotype IgM BF-F3 against MYH4 (Hybridoma Bank, University of Iowa), mouse monoclonal isotype IgM 6H1 against MYH1 (Hybridoma Bank, University of Iowa), mouse monoclonal isotype IgG1 BF-B6 against MYH8 (kind gift of Dr. Gary Coulton), mouse monoclonal isotype IgG1 CPTC-CRYAB-3-s against a/b-crystallin (Hybridoma Bank, University of Iowa) and mouse monoclonal against α-actinin (EA-53, SIGMA). All monoclonal antibodies were used at dilution 1:20.

Next generation sequencing

Hybrid selection with long oligonucleotides in solution (40) was used to enrich for every annotated exon in the *ariel* non-recombinant interval (Ensembl release 50). The sequences of all annotated exons were used to design 120 nt oligonucleotides. The oligonucleotides were synthesized and converted into RNA 'baits' (Agilent SureSelect). Genomic DNAs from an *ariel* homozygous mutant was converted into Illumina sequencing libraries (Geneservice, UK) and the RNA baits

Downloaded from https://academic.oup.com/hmg/article/21/8/1706/621832 by guest on 13 March 2024

then used to capture exon fragments from the sequencing libraries by hybridization. Sequencing was done using the Illumina GA2 platform (Geneservice) to produce 36-base reads. Each flow cell lane produced 200–300 Mb of raw data that passed Illumina quality filters. The error rate of the Illumina sequencing method is 2%. All exon–intron boundaries were covered, and the average read depth over the whole candidate region was 37.

Single-end sequence reads (36mers) were aligned to the reference C57BL/6J sequence using Maq (http://sourceforge.net/projects/maq/). The default alignment parameters were used with up to two mismatches and a consensus sequence generated. Identification of homozygous SNPs was carried out with Maq and unreliable SNPs were filtered using Maq's in-built SNP filter. Unique SNPs were identified in two ways. First, inbred SNPs for C57BL/6J recorded in NCBI's dbSNP (41) and the 17 Genomes project (http://www.sanger.ac.uk/resources/mouse/genomes/) were filtered out and, secondly, SNPs previously predicted in MRC Harwell's C57BL/6J strain were also eliminated. Putative sequence variants were validated by PCR and Sanger sequencing of independent mutant DNAs.

qPCR analysis

Muscle samples from the hindlimbs (gastrocnemius muscles) from homozygous ($n = 5$), heterozygous ($n = 3$) and wild type ($n = 4$) were dissected from 13-day-old freshly killed mice and immediately frozen on dry ice. Total RNA was extracted and DNase treated using RNeasy lipid midi kit (Qiagen) following manufacture's recommendations. The quantity of the RNA was checked using a Nanodrop ND1000 and the integrity assessed by gel electrophoresis. Assays were designed that would distinguish between the mutant and wild-type Ariel allele using Biosearch Technologies software (http://www.biosearchtech.com/). The same forward and reverse primers were used for both alleles; the sequences are as follows:

Forward primer: GCTGATGGCCACAGACACT
Reverse primer: AGCGCCTGTGAGCTTGTAAATGG

Probes were designed for each specific allele; the sequences are as follows (underlined letter discriminates the mutation):

Mutant-probe: CTGTTGATATCCAGGGA
Wild type-probe: CTGTTGATATCCTGGGA

Double-stranded cDNA was synthesized from 2 μg total RNA using High Capacity cDNA Archive kit from Applied Biosystems. Quantitative real-time PCR was performed using Applied Biosystems TaqMan® Gene Expression Assays, using TaqMan® Fast Universal PCR Master Mix on a 7500 Fast Real-Time PCR System (Applied Biosystems). Ten nanograms of cDNA were used as template to determine the relative amounts of mRNA in each assay. Gapdh was used as the endogenous control (catalogue number Mm99999915-g1), and PCR and cycling conditions were set following manufacture's recommendations.

Statistical analysis was performed using a two-tailed Student's *t*-test.

Constructs

A full-length mouse *Myh4* cDNA was available as an IMAGE clone (ID 9055974, vector pCR-XL-TOPO). We used this clone as template to generate the *ariel* mutation by site-directed mutagenesis (Phusion™ Site-Directed Mutagenesis Kit, Finnzymes). Once verified by sequencing, mutant and control *Myh4* cDNAs were amplified by high-fidelity PCR and cloned into the expression vector pcDNA3.1/CT-GFP-TOPO (Invitrogen) to the express GFP-tagged versions referred to as MYH4:GFP and MYH4^{L342Q}:GFP. The pcDNA3.1/CT-MYH4:GFP construct was also modified to generate an MYH4:tdTomato version. For this, the tdTomato tag was amplified by PCR from the pRSET-B_tdTomato vector (kind gift of Dr. Paul Pryor) and cloned into the pcDNA3.1/CT-MYH4:GFP using the In-Fusion method (Clontech), following manufacturer instructions. pcDNA3.1/CT-MYH4:GFP was previously linearized with *Nhe*I and *Bst*BI (New England Biolabs) and gel purified to eliminate the GFP tag. A full-length human *Myh1* cDNA (FL25691, vector pCR-BluntII-TOPO) was available from LabOmics (Belgium). The full-length *Myh1* cDNA was amplified and re-cloned into the vector pcDNA3.1/CT-GFP-TOPO and a version containing the *ariel* mutation generated by site-directed mutagenesis, using the methods as described above for *Myh4*.

In vitro expression and quantifications

COS7 cells were grown on DMEM medium (Sigma) supplemented with antibiotics and L-glutamine and 15% bovine serum. Cells were transfected using FuGENE 6 according to the manufacturer's instructions (Roche). After 48 h, cells were fixed with 6% paraformaldehyde and washed twice with PBS. All fluorescence images were captured using a Zeiss Axiophot fluorescent microscope or a Leica TCS SP5 confocal microscope, using LAS AF software (Leica). Four independent transfections were performed, and cells were counted and classified according to the presence/absence of inclusions (see Fig. 4A). The results were statistically treated to produce the graph shown in Figures 4A and 10. In the case of C2C12s, cells were plated on collagen-coated dishes. At 70% of confluence, cells were transfected and allowed to differentiate after reaching confluency by switching to a low serum medium (2%).

Muscle sampling and fibre permeabilization

EDL muscles were placed in relaxing solution at 4°C. Bundles of ~50 fibres were dissected free and then tied with surgical silk to glass capillary tubes at slightly stretched lengths. They were then treated with skinning solution (relaxing solution containing glycerol; 50:50 v/v) for 24 h at 4°C, after which they were transferred to −20°C. In addition, the muscle bundles were treated with sucrose, a cryoprotectant, within 1–2 weeks for long-term storage. They were detached from the capillary tubes and snap frozen in liquid nitrogen-chilled propane and stored at −160°C. On the day of experiment, bundles were de-sucrosed by stepwise lowering the sucrose concentration of the relax solution, transferred to a

Downloaded from https://academic.oup.com/hmg/article/21/8/1706/621832 by guest on 13 March 2024

relaxing solution and single fibres dissected. A fibre segment 1–2 mM long was left between connectors leading to a force transducer (model 400A, Aurora Scientific) and a lever arm system (model 308B, Aurora Scientific). The apparatus was mounted on the stage of an inverted microscope (model IX70; Olympus). The sarcomere length was set to 2.50 μm and controlled during the experiment using a high-speed video analysis system (model 901A HVSL, Aurora Scientific). The diameter of the fibre between the connectors was measured through the microscope at a magnification of ×320 with an image analysis system prior to the mechanical experiments. Fibre depth was measured by recording the vertical displacement of the microscope nosepiece while focusing on the top and bottom surfaces of the fibre. The focusing control of the microscope was used as a micrometer. The cross-sectional area was calculated from the diameter and depth, assuming an elliptical circumference, and was corrected for the 20% swelling that is known to occur during skinning. At 15°C, maximal force generation was calculated as the difference between the steady-state isometric force in activating solution and the resting force measured in the same segment while in the relaxing solution. Maximal force was adjusted for the cross-sectional area. In addition, during steady-state isometric force production, a slack by 20% of the original fibre length was rapidly introduced (within 1–2 ms) at one end of the fibre, resulting in a rapid reduction of force to near zero. This was followed by a brief period of unloaded shortening (20 ms), after which the preparation was quickly re-stretched to its original length and the force was recovered to its original steady-state value. The rate of force development was estimated by linear transformation of the half-time of force redevelopment. After the contractile measurements, each fibre was placed in urea buffer (120 g urea, 38 g thiourea, 70 ml H_2O, 25 g mixed bed resin, 2.89 g dithiothreitol, 1.51 g Trizma base, 7.5 g SDS, 0.004% bromophenol blue) in a plastic microcentrifuge tube and stored at −80°C.

Protein isoform expression. The MyHC isoform composition of single fibres was determined by 6% SDS–PAGE. The acrylamide concentration was 4% (wt/vol) in the stacking gel and 6% in the running gel, and the gel matrix included 30% glycerol. Sample loads were kept small (equivalent to ∼0.05 mM of fibre segment) to improve the resolution of the MyHC bands (types I, IIa, IIx and IIb). Electrophoresis was performed at 120 V for 24 h with a Tris–glycine electrode buffer (pH 8.3) at 15°C (SE 600 vertical slab gel unit, Hoefer Scientific Instruments). The gels were silver stained and subsequently scanned in a soft laser densitometer (Molecular Dynamics) with a high spatial resolution (50 μm pixel spacing) and 4096 optical density levels.

Solutions. Relaxing and activating solutions contained (in mM) 4 Mg-ATP, 1 free Mg^{2+}, 20 imidazole, 7 EGTA, 14.5 creatine phosphate and KCl to adjust the ionic strength to 180 mM. The pH was adjusted to 7.0. The concentrations of free Ca^{2+} were 10^{-9} M (relaxing solution) and $10^{-4.5}$ M (activating solution), expressed as pCas (i.e. $-\log [Ca^{2+}]$). Apparent stability constants for Ca^{2+}–EGTA were corrected for temperature (15°C) and ionic strength (180 mM). The computer program of Fabiato was used to calculate the concentrations of each metal, ligand and metal–ligand complex.

Statistical analysis. Data are presented as means ± standard error of the means (SEM). Sigma Stat software (Jandel Scientific) was used to generate descriptive statistics. Comparisons were restricted to fibres expressing the type IIb MyHC isoform. To evaluate the effects of the mutation on contractility, the unpaired Student's *t*-test was applied.

Laser microdissection of Ariel inclusions

Twenty-micrometre sections of frozen Ariel and C57BL/10 (BL/10) control muscle were collected on membrane slides (Leica Microsystems, Frankfurt, Germany) and subsequently stained with a standard H&E protocol, slightly modified by reducing staining times for eosin and increasing wash steps. Eight hundred Ariel inclusions and 500 BL/10 control fibres (estimated total proteins of 650 ng per dataset) were isolated via laser microdissection (LMD 7000, Leica Microsystems) and collected in separate, sterile, 0.5 ml PCR tubes. The material was stored at −80°C.

Mass spectroscopy

The PINNACLE group (Newcastle, UK) analysed captured materials via mass spectroscopy using a Thermo-Finnegan LTQ mass spectrometer, concatenated MS/MS data from triplicate runs into a single data submission file and searched these against the NCBInr protein database. The list of proteins presented were those with two or more peptide matches and a Mascot score above the 95% cut-off and they were ranked according to their reliability.

Analysis of MS/MS data

Proteomic analysis identified 56 different proteins in Ariel inclusions and 41 in BL/10 control fibres with a *P*-value of <0.05. Proteins were ranked according to their individual ion score, which is based on the number of peptide matches. Although this ranking system is not quantitative, some correlation can be assumed between the quantity of a peptide and its specificity.

Quantifications of MYH4 and MYH4^{L342Q}

The levels of mutant and wild-type myosins were quantified by LC-MS essentially as described in (42) using a nanoAcquity HPLC (Waters, Milford, Massachusetts, USA) and a maXis high-resolution mass spectrometer (Bruker, Bremen, Germany). Labelled peptide standards corresponding to amino acid residues 332–349 of MYH4 containing wild-type and mutant sequence, differing only in residue 342, LMATDTAVDIQG[$U^{13}C_9$, ^{15}N–F]SADEK and LMATD TAVDILG[$U^{13}C_9$, ^{15}N–F]SADEK, were synthesized and assayed by amino acid analysis by Cambridge Research Biochemicals (Cleveland, UK). Muscle protein was proteolytically digested with a combination of sequencing-grade, porcine trypsin (Promega, Madison, WI, USA) and endoproteinase Glu-C from *Staphylococcus aureus* (Sigma, St. Louis, MO,

Downloaded from https://academic.oup.com/hmg/article/21/8/1706/621832 by guest on 13 March 2024

USA). Eight different amounts of each labelled peptide (from 0.5 to 500 fmol) were added to equal volumes of the proteolytic digest. Prior to LC–MS, methionine residues were oxidized in 3% (v/v) H_2O_2 for 30 min at 30°C to eliminate the splitting of ion intensity between the oxidized and un-oxidized forms of the peptides. Calibration curves for the two labelled peptides were derived from ion intensities obtained from extracted ion chromatograms of their doubly protonated ions—*m/z* 961.980 for the wild-type peptide and *m/z* 969.467 for the mutant peptide. Intensities of the native, unlabelled peptides in the eight samples were used to determine the amounts of mutant and wild-type protein from the calibration curves. In order to accommodate the order of magnitude difference between the amounts of mutant and wild-type peptide present in the muscle samples, two different calibration curves were used (see Supplementary Material, Fig. S1).

SUPPLEMENTARY MATERIAL

Supplementary Material is available at *HMG* online.

ACKNOWLEDGEMENTS

We would like to acknowledge Dr Jerry Thomas and Dr David Ashford from the Technology Facility (Biology Department, York University) for their pivotal contribution to the myosin quantifications performed in this work.

Conflict of Interest statement. None declared.

FUNDING

This work was funded by the UK Medical Research Council and the Biology Department, University of York, UK (to G.B.).

REFERENCES

1. Schroder, R. and Schoser, B. (2009) Myofibrillar myopathies: a clinical and myopathological guide. *Brain Pathol.*, **19**, 483–492.
2. Ferrer, I. and Olive, M. (2008) Molecular pathology of myofibrillar myopathies. *Expert Rev. Mol. Med.*, **10**, e25.
3. Olive, M. (2009) Extralysosomal protein degradation in myofibrillar myopathies. *Brain Pathol.*, **19**, 507–515.
4. Selcen, D. (2008) Myofibrillar myopathies. *Curr. Opin. Neurol.*, **21**, 585–589.
5. Bohlega, S., Lach, B., Meyer, B.F., Al Said, Y., Kambouris, M., Al Homsi, M. and Cupler, E.J. (2003) Autosomal dominant hyaline body myopathy: clinical variability and pathologic findings. *Neurology*, **61**, 1519–1523.
6. Martinsson, T., Darin, N., Kyllerman, M., Oldfors, A., Hallberg, B. and Wahlstrom, J. (1999) Dominant hereditary inclusion-body myopathy gene (IBM3) maps to chromosome region 17p13.1. *Am. J. Hum. Genet.*, **64**, 1420–1426.
7. Martinsson, T., Oldfors, A., Darin, N., Berg, K., Tajsharghi, H., Kyllerman, M. and Wahlstrom, J. (2000) Autosomal dominant myopathy: missense mutation (Glu-706 → Lys) in the myosin heavy chain IIa gene. *Proc. Natl Acad. Sci. USA*, **97**, 14614–14619.
8. Darin, N., Kyllerman, M., Wahlstrom, J., Martinsson, T. and Oldfors, A. (1998) Autosomal dominant myopathy with congenital joint contractures, ophthalmoplegia, and rimmed vacuoles. *Ann. Neurol.*, **44**, 242–248.
9. Shingde, M.V., Spring, P.J., Maxwell, A., Wills, E.J., Harper, C.G., Dye, D.E., Laing, N.G. and North, K.N. (2006) Myosin storage (hyaline body) myopathy: a case report. *Neuromuscul. Disord.*, **16**, 882–886.
10. Tajsharghi, H., Thornell, L.E., Lindberg, C., Lindvall, B., Henriksson, K.G. and Oldfors, A. (2003) Myosin storage myopathy associated with a heterozygous missense mutation in MYH7. *Ann. Neurol.*, **54**, 494–500.
11. Goebel, H.H. and Muller, H.D. (2006) Protein aggregate myopathies. *Semin. Pediatr. Neurol.*, **13**, 96–103.
12. Tajsharghi, H., Oldfors, A., Macleod, D.P. and Swash, M. (2007) Homozygous mutation in MYH7 in myosin storage myopathy and cardiomyopathy. *Neurology*, **68**, 962.
13. Blair, E., Redwood, C., de Jesus Oliveira, M., Moolman-Smook, J.C., Brink, P., Corfield, V.A., Ostman-Smith, I. and Watkins, H. (2002) Mutations of the light meromyosin domain of the beta-myosin heavy chain rod in hypertrophic cardiomyopathy. *Circ. Res.*, **90**, 263–269.
14. Tajsharghi, H., Hilton-Jones, D., Raheem, O., Saukkonen, A.M., Oldfors, A. and Udd, B. (2010) Human disease caused by loss of fast IIa myosin heavy chain due to recessive MYH2 mutations. *Brain*, **133**, 1451–1459.
15. Acakpo-Satchivi, L.J., Edelmann, W., Sartorius, C., Lu, B.D., Wahr, P.A., Watkins, S.C., Metzger, J.M., Leinwand, L. and Kucherlapati, R. (1997) Growth and muscle defects in mice lacking adult myosin heavy chain genes. *J. Cell Biol.*, **139**, 1219–1229.
16. Sartorius, C.A., Lu, B.D., Acakpo-Satchivi, L., Jacobsen, R.P., Byrnes, W.C. and Leinwand, L.A. (1998) Myosin heavy chains IIa and IId are functionally distinct in the mouse. *J. Cell Biol.*, **141**, 943–953.
17. Allen, D.L., Harrison, B.C., Sartorius, C., Byrnes, W.C. and Leinwand, L.A. (2001) Mutation of the IIB myosin heavy chain gene results in muscle fiber loss and compensatory hypertrophy. *Am. J. Physiol. Cell Physiol.*, **280**, C637–645.
18. Allen, D.L. and Leinwand, L.A. (2001) Postnatal myosin heavy chain isoform expression in normal mice and mice null for IIb or IId myosin heavy chains. *Dev. Biol.*, **229**, 383–395.
19. Margossian, S.S. and Lowey, S. (1973) Substructure of the myosin molecule. IV. Interactions of myosin and its subfragments with adenosine triphosphate and F-actin. *J. Mol. Biol.*, **74**, 313–330.
20. Mornet, D., Pantel, P., Audemard, E. and Kassab, R. (1979) The limited tryptic cleavage of chymotryptic S-1: an approach to the characterization of the actin site in myosin heads. *Biochem. Biophys. Res. Commun.*, **89**, 925–932.
21. Rayment, I., Rypniewski, W.R., Schmidt-Base, K., Smith, R., Tomchick, D.R., Benning, M.M., Winkelmann, D.A., Wesenberg, G. and Holden, H.M. (1993) Three-dimensional structure of myosin subfragment-1: a molecular motor. *Science*, **261**, 50–58.
22. Geeves, M.A. and Holmes, K.C. (1999) Structural mechanism of muscle contraction. *Annu. Rev. Biochem.*, **68**, 687–728.
23. Agbulut, O., Noirez, P., Beaumont, F. and Butler-Browne, G. (2003) Myosin heavy chain isoforms in postnatal muscle development of mice. *Biol. Cell*, **95**, 399–406.
24. Lucas, C.A., Kang, L.H. and Hoh, J.F. (2000) Monospecific antibodies against the three mammalian fast limb myosin heavy chains. *Biochem. Biophys. Res. Commun.*, **272**, 303–308.
25. van Spaendonck-Zwarts, K., van Hessem, L., Jongbloed, J.D., de Walle, H.E., Capetanaki, Y., van der Kooi, A.J., van Langen, I.M., van den Berg, M.P. and van Tintelen, J.P. (2011) Desmin-related myopathy: a review and meta-analysis. *Clin Genet.*, **80**, 354–366.
26. Selcen, D. and Engel, A.G. (2003) Myofibrillar myopathy caused by novel dominant negative alpha B-crystallin mutations. *Ann. Neurol.*, **54**, 804–810.
27. Vicart, P., Caron, A., Guicheney, P., Li, Z., Prevost, M.C., Faure, A., Chateau, D., Chapon, F., Tome, F., Dupret, J.M. *et al.* (1998) A missense mutation in the alphaB-crystallin chaperone gene causes a desmin-related myopathy. *Nat. Genet.*, **20**, 92–95.
28. Smerdu, V., Karsch-Mizrachi, I., Campione, M., Leinwand, L. and Schiaffino, S. (1994) Type IIx myosin heavy chain transcripts are expressed in type IIb fibers of human skeletal muscle. *Am. J. Physiol.*, **267**, C1723–1728.
29. Jansen, G., Groenen, P.J., Bachner, D., Jap, P.H., Coerwinkel, M., Oerlemans, F., van den Broek, W., Gohlsch, B., Pette, D., Plomp, J.J. *et al.* (1996) Abnormal myotonic dystrophy protein kinase levels produce only mild myopathy in mice. *Nat. Genet.*, **13**, 316–324.
30. Risal, D., Gourinath, S., Himmel, D.M., Szent-Gyorgyi, A.G. and Cohen, C. (2004) Myosin subfragment 1 structures reveal a partially bound

Downloaded from https://academic.oup.com/hmg/article/21/8/1706/621832 by guest on 13 March 2024

nucleotide and a complex salt bridge that helps couple nucleotide and actin binding. *Proc. Natl Acad. Sci. USA*, **101**, 8930–8935.
31. Holmes, K.C., Angert, I., Kull, F.J., Jahn, W. and Schroder, R.R. (2003) Electron cryo-microscopy shows how strong binding of myosin to actin releases nucleotide. *Nature*, **425**, 423–427.
32. Himmel, D.M., Gourinath, S., Reshetnikova, L., Shen, Y., Szent-Gyorgyi, A.G. and Cohen, C. (2002) Crystallographic findings on the internally uncoupled and near-rigor states of myosin: further insights into the mechanics of the motor. *Proc. Natl Acad. Sci. USA*, **99**, 12645–12650.
33. Coureux, P.D., Wells, A.L., Menetrey, J., Yengo, C.M., Morris, C.A., Sweeney, H.L. and Houdusse, A. (2003) A structural state of the myosin V motor without bound nucleotide. *Nature*, **425**, 419–423.
34. Kohler, J., Winkler, G., Schulte, I., Scholz, T., McKenna, W., Brenner, B. and Kraft, T. (2002) Mutation of the myosin converter domain alters cross-bridge elasticity. *Proc. Natl Acad. Sci. USA*, **99**, 3557–3562.
35. Keller, D.I., Coirault, C., Rau, T., Cheav, T., Weyand, M., Amann, K., Lecarpentier, Y., Richard, P., Eschenhagen, T. and Carrier, L. (2004) Human homozygous R403W mutant cardiac myosin presents disproportionate enhancement of mechanical and enzymatic properties. *J. Mol. Cell Cardiol.*, **36**, 355–362.
36. Belus, A., Piroddi, N., Scellini, B., Tesi, C., Amati, G.D., Girolami, F., Yacoub, M., Cecchi, F., Olivotto, I. and Poggesi, C. (2008) The familial hypertrophic cardiomyopathy-associated myosin mutation R403Q accelerates tension generation and relaxation of human cardiac myofibrils. *J. Physiol.*, **586**, 3639–3644.
37. Seebohm, B., Matinmehr, F., Kohler, J., Francino, A., Navarro-Lopez, F., Perrot, A., Ozcelik, C., McKenna, W.J., Brenner, B. and Kraft, T. (2009) Cardiomyopathy mutations reveal variable region of myosin converter as major element of cross-bridge compliance. *Biophys. J.*, **97**, 806–824.
38. Soto, C. (2001) Protein misfolding and disease; protein refolding and therapy. *FEBS Lett.*, **498**, 204–207.
39. Horton, M.J., Brandon, C.A., Morris, T.J., Braun, T.W., Yaw, K.M. and Sciote, J.J. (2001) Abundant expression of myosin heavy-chain IIB RNA in a subset of human masseter muscle fibres. *Arch. Oral Biol.*, **46**, 1039–1050.
40. Gnirke, A., Melnikov, A., Maguire, J., Rogov, P., LeProust, E.M., Brockman, W., Fennell, T., Giannoukos, G., Fisher, S., Russ, C. *et al.* (2009) Solution hybrid selection with ultra-long oligonucleotides for massively parallel targeted sequencing. *Nat. Biotechnol.*, **27**, 182–189.
41. Sherry, S.T., Ward, M.H., Kholodov, M., Baker, J., Phan, L., Smigielski, E.M. and Sirotkin, K. (2001) dbSNP: the NCBI database of genetic variation. *Nucleic Acids Res.*, **29**, 308–311.
42. Becker, E., Navarro-Lopez, F., Francino, A., Brenner, B. and Kraft, T. (2007) Quantification of mutant versus wild-type myosin in human muscle biopsies using nano-LC/ESI-MS. *Anal Chem.*, **79**, 9531–9538.
43. Kabsch, W. and Sander, C. (1983) Dictionary of protein secondary structure: pattern recognition of hydrogen-bonded and geometrical features. *Biopolymers*, **22**, 2577–2637.
44. Hogue, C.W. (1997) Cn3D: a new generation of three-dimensional molecular structure viewer. *Trends Biochem. Sci.*, **22**, 314–316.

Downloaded from https://academic.oup.com/hmg/article/21/8/1706/621832 by guest on 13 March 2024